Oncogene (2021) 40:1091–1105
https://doi.org/10.1038/s41388-020-01584-6

ARTICLE

STAT3 promotes melanoma metastasis by CEBP-induced repression of the MITF pathway

Alexander Swoboda[1,2] · Robert Soukup[3] · Oliver Eckel[2,3] · Katharina Kinslechner[3] · Bettina Wingelhofer[1,2] · David Schörghofer[3] · Christina Sternberg[4] · Ha T. T. Pham[1,2] · Maria Vallianou[3] · Jaqueline Horvath[1,5] · Dagmar Stoiber[1,5] · Lukas Kenner[1,6,7,8] · Lionel Larue[9] · Valeria Poli[10] · Friedrich Beermann[11] · Takashi Yokota[12] · Stefan Kubicek[13] · Thomas Krausgruber[13] · André F. Rendeiro[13] · Christoph Bock[13,14,15] · Rainer Zenz[16] · Boris Kovacic[3] · Fritz Aberger[4] · Markus Hengstschläger[3] · Peter Petzelbauer[17] · Mario Mikula[3] · Richard Moriggl[1,2]

Received: 19 February 2020 / Revised: 30 October 2020 / Accepted: 24 November 2020 / Published online: 15 December 2020

Abstract

Metastatic melanoma is hallmarked by its ability of phenotype switching to more slowly proliferating, but highly invasive cells. Here, we tested the impact of signal transducer and activator of transcription 3 (STAT3) on melanoma progression in association with melanocyte inducing transcription factor (MITF) expression levels. We established a mouse melanoma model for deleting *Stat3* in melanocytes with specific expression of human hyperactive $NRAS^{Q61K}$ in an *Ink4a*-deficient background, two frequent driver mutations in human melanoma. Mice devoid of *Stat3* showed early disease onset with higher proliferation in primary tumors, but displayed significantly diminished lung, brain, and liver metastases. Whole-genome expression profiling of tumor-derived cells also showed a reduced invasion phenotype, which was further corroborated by 3D melanoma model analysis. Notably, loss or knockdown of *STAT3* in mouse or human cells resulted in the upregulation of MITF and induction of cell proliferation. Mechanistically we show that STAT3-induced *CAAT Box Enhancer Binding Protein* (*CEBP*) expression was sufficient to suppress *MITF* transcription. Epigenetic analysis by ATAC-seq confirmed that *CEBPa/b* binding to the *MITF* enhancer region silenced the *MITF* locus. Finally, by classification of patient-derived melanoma samples, we show that STAT3 and MITF act antagonistically and hence contribute differentially to melanoma progression. We conclude that STAT3 is a driver of the metastatic process in melanoma and able to antagonize *MITF* via direct induction of CEBP family member transcription.

Introduction

Melanoma is a very aggressive form of skin cancer, with >76,000 new cases diagnosed annually in the USA [1]. Stage I and stage II lesions can be successfully removed by surgery, but metastasized melanomas are challenging to treat, leading to an estimated 10,000 deaths in the USA annually [1]. The current prognosis of advanced melanoma remains poor despite the success of immune- and targeted therapy. The plasticity of melanoma, which describes the ability of melanoma cells to switch multiple times from a proliferative to an invasive state and vice versa without the need for additional mutations, is in part responsible for the low curation rates [2, 3]. This process is also called phenotype switching and involves the melanocyte inducing transcription factor (MITF) [4]. MITF is essential for melanocyte development, homeostasis, and pigmentation response [5, 6]. MITF controls differentiation, survival, and proliferation and its expression is also transcriptionally regulated by SOX10, a transcriptional activator important for neural crest development [7]. High MITF expression

These authors contributed equally: Alexander Swoboda, Robert Soukup

Supplementary information The online version of this article (https://doi.org/10.1038/s41388-020-01584-6) contains supplementary material, which is available to authorized users.

✉ Mario Mikula
mario.mikula@meduniwien.ac.at

✉ Richard Moriggl
richard.moriggl@vetmeduni.ac.at

Extended author information available on the last page of the article

marks melanoma cells with a proliferative, but noninvasive phenotype. In contrast, melanoma cells expressing low MITF protein represent increased invasive and metastatic capacity [2, 8–10]. These findings exemplify an essential role for MITF in melanoma biology.

Although the transcriptional regulation of MITF is well described, the interplay with signal transducer and activator of transcription 3 (STAT3) in cancer biology has so far not been established. STAT3 shows enhanced tyrosine phosphorylation in melanoma, catalyzed via JAK, SRC, or growth factor tyrosine kinase family members [11]. Reports on inhibition of STAT3 by siRNA or expression of a dominant negative form of STAT3 in melanoma xenografts postulated an oncogenic role of STAT3 in melanoma progression [12, 13]. However, treatment with STAT3 activators like oncostatin M (OSM) or IL-6 resulted in tyrosine phosphorylation of STAT3 and decreased proliferation in melanoma cell line studies, suggesting a tumor suppressor role for STAT3 in melanoma progression [14, 15]. Complete genetic deletion studies for STAT3 in melanoma are still missing, whereas in prostate, lung and colorectal carcinomas, tumor suppressive roles were associated with STAT3 function depending on the mutational context [16–18]. Importantly, it is not clear whether STAT3 plays a role in phenotype switching toward invasive melanoma.

Here, we utilized a genetic model of spontaneous melanoma formation based on relevant driver mutations for human melanoma initiation and progression. Mice carrying melanocyte-specific expression of the $NRAS^{Q61K}$ oncogene in an *Ink4a*-deficient background were generated [19, 20]. Additionally, our mouse model allows for conditional melanocyte-specific deletion of *Stat3* [21]. We show that mice lacking *Stat3* expression in melanomas have an accelerated visible tumor onset in vivo and exert a higher proliferating cell nuclear antigen (PCNA) labeling. In contrast, metastasis formation from *Stat3* knockout primary tumors was severely impaired when analyzing lung, brain and liver tissue. Next, STAT3 function was evaluated mechanistically using tumor-derived cell lines, where we performed whole-genome expression analysis combined with ATAC-seq profiling. We found, that STAT3 antagonizes MITF expression through elevated expression of CAAT Box Enhancer Binding Protein (CEBP) family members. Remarkably, in silico data mining of melanoma patient samples also revealed a negative correlation of *CEBPa/b* with *MITF* mRNA expression values. *STAT3* knockdowns in human melanoma confirmed the antagonistic action on MITF expression with consequences for changed proliferation and invasion. We conclude that loss or downregulation of STAT3 inhibits melanoma metastasis and that in response MITF is upregulated. We propose that the complex interplay of these two master regulators, which both act as oncogenes in melanoma progression, determines clinical outcome and patient fate.

Results

Tissue-specific loss of STAT3 enabled earlier tumor onset

To study the effect of STAT3 loss in melanoma, we used transgenic mice that allow for conditional deletion of *Stat3* by C*re-loxP* technology. To closely mimic human cutaneous melanoma progression, we employed a genetic mouse model driven by melanocyte-specific hyperactive human $NRAS^{Q61K}$ that has been further crossed to an *INK4a*-deficient background. Melanoma that carry $NRAS^{Q61K}$, lost $p16^{INK4A}$ and $p19^{ARF}$, and deleted *Stat3* (Tyr::$NRAS^{Q61K}$$Ink4a^{-/-}$$Stat3^{flox/flox}$Tyr::Cre) are further termed $Stat3^{\Delta}$, control melanoma expressing STAT3 are termed $Stat3^{fl}$ (Fig. 1A). Melanocyte-specific CRE expression was described to recombine *loxP* sites from E10.5 onwards in development [22]. Consistently, mice developed tumors on their skin starting from 12 weeks of age (Fig. 1B). Disease onset, defined as appearance of palpable tumors with a size bigger than 1 mm, was significantly accelerated in the $Stat3^{\Delta}$ group (Fig. 1C).

As expected, STAT3 was lost in mouse skin melanomas when tested by immunohistochemistry (Fig. 1D). PCNA staining revealed that primary $Stat3^{\Delta}$ tumors displayed increased proliferative activity compared to $Stat3^{fl}$ tumors (Fig. 1E). Loss of *Stat3* could affect expression from the *Stat5a* and *Stat5b* gene locus, which resides in proximity on the same chromosome. Hence, we further investigated their expression and nuclear localization by antibody staining, but no significant difference was observed (Supplementary Fig. S2a, b).

Expression profiling revealed pigmentation and MITF pathway induction upon loss of STAT3

We isolated tumor cells from melanoma positive lymph nodes of the $Stat3^{fl}$ and $Stat3^{\Delta}$ mice and selected for melanoma cells by continuous culturing. Cells were uniformly positive for the melanoma marker S100b (Supplementary Fig. S2c). Control cells showed basic STAT3 activity according to Y705 phosphorylation, while with IL-6 stimulation enhanced STAT3 activity was observed (Fig. 2A). Importantly, $Stat3^{\Delta}$ cells showed complete loss of STAT3 expression and STAT3 Y705 phosphorylation in all conditions as detected by western blotting.

Next, we performed Affymetrix whole-transcriptome microarray mRNA analysis followed by gene-set enrichment analysis (GSEA) under basal growth conditions or during stimulation with murine IL-6 or OSM. Loss of *Stat3* resulted in significant reduction of STAT3 target gene expression and importantly, $Stat3^{\Delta}$ cells displayed augmented MITF pathway activation (Fig. 2B). As expected

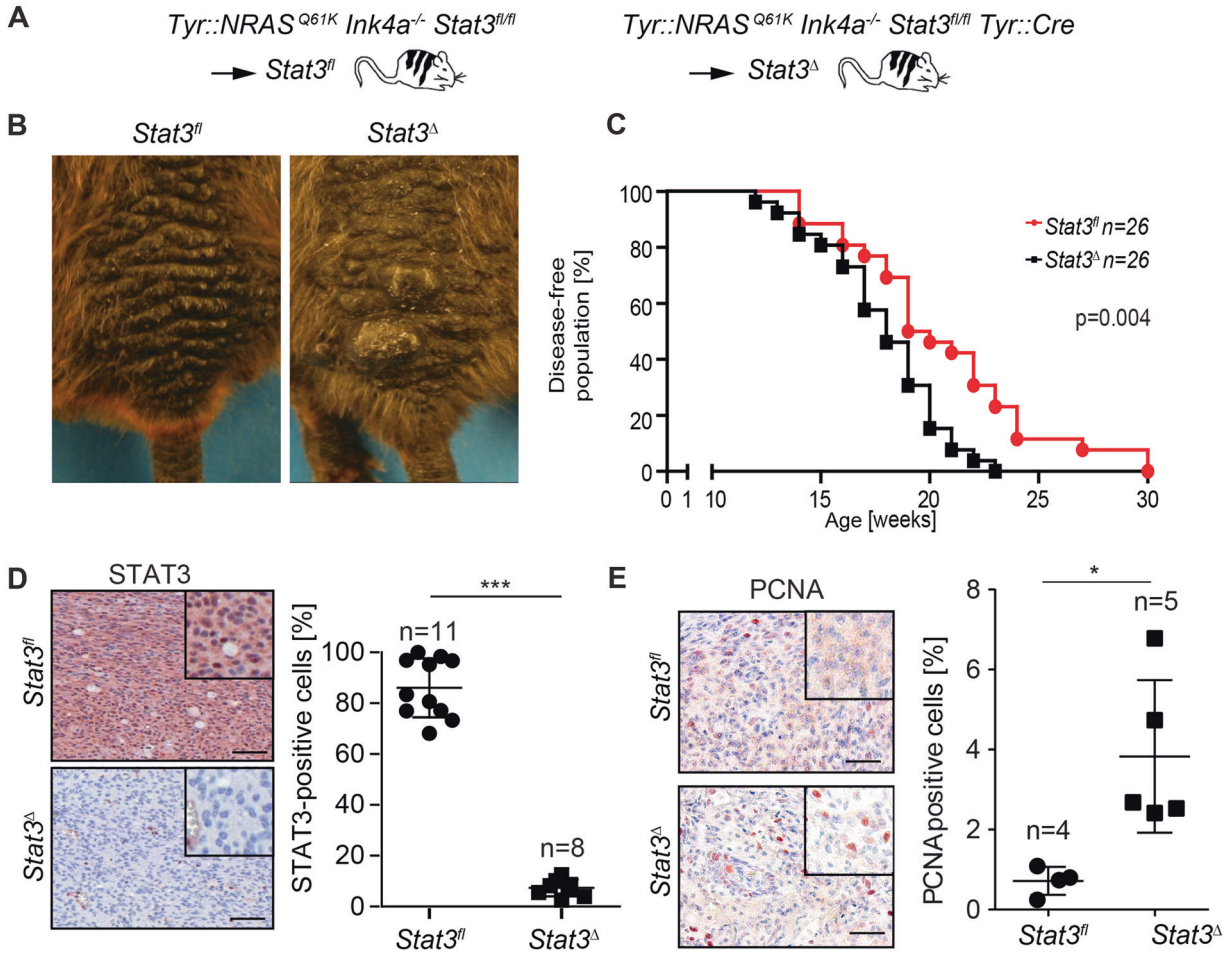

Fig. 1 STAT3 knockout in melanoma induced earlier tumor onset, but reduced metastasis. A Mice containing a constitutively active *NRAS* gene controlled by the *tyrosinase* promoter and a deletion of the *Ink4a* locus were crossed to mice harboring a *floxed Stat3* locus termed "Stat3^{fl}." Mice additionally expressing *Cre* recombinase by a *tyrosinase* promoter were termed "Stat3$^{\Delta}$." **B** Representative pictures of 20-week-old mice. **C** Logrank (Mantel-Cox) test was used to display Kaplan–Meier plot, showing disease-free survival, defined as time before palpable tumors occur, of Stat3^{fl} mice compared to the Stat3$^{\Delta}$ group. **D**, **E** IHC evaluation of total STAT3 and PCNA in primary melanoma of Stat3^{fl} and Stat3$^{\Delta}$ mice. Scale bars, 50 µm. Data are shown as mean ± SD. *P* values represent Mann–Whitney *U* test. $*P < 0.05$; $***P < 0.001$.

cytokine stimulation had no effect on STAT3 target or MITF pathway gene expression in knockdown cells (Fig. 2C, D and Supplementary Fig. S3a–c). Increased MITF activity was validated by measuring absorbance of melanin in conditioned medium of STAT3 wild type and knockout cells (Fig. 2E). Additionally we detected increased melanin amounts in primary tumors lacking *Stat3* (Fig. 2F). We conclude that the loss of *Stat3* is accompanied by the upregulation of the MITF pathway resulting in increased pigmentation of cells and tissue.

Invasion and metastatic outcome are reduced upon loss of *Stat3*

GSEA, including proliferative and invasive melanoma signatures, were performed to identify STAT3-related phenotypes (Fig. 3A). We found that Stat3$^{\Delta}$ cells resembled MITF-driven proliferative gene signatures, which were identified in two large and independent melanoma cohort studies [2, 10, 23, 24]. In contrast, Stat3^{fl} cells were closely related to the described invasive signatures [10, 23] and the hallmark EMT data set defined by the GSEA team [25].

To validate our whole-genome expression profiling, we performed in vitro assays, where we found enhanced 3D proliferation, but abrogated invasion and migration in Stat3$^{\Delta}$ cells (Fig. 3B, C). Our data imply that STAT3 fulfills an important function in RAS-transformed melanoma promoting invasion and migration. Tumor allografts of Stat3$^{\Delta}$ cells were more compact, with higher cellular density and allografts showed little to no significant invasion of epidermal tissue. In contrast, Stat3^{fl}-derived tumors were dedifferentiated with fibroblastoid morphology, displaying high invasion into murine epidermis (Fig. 3D).

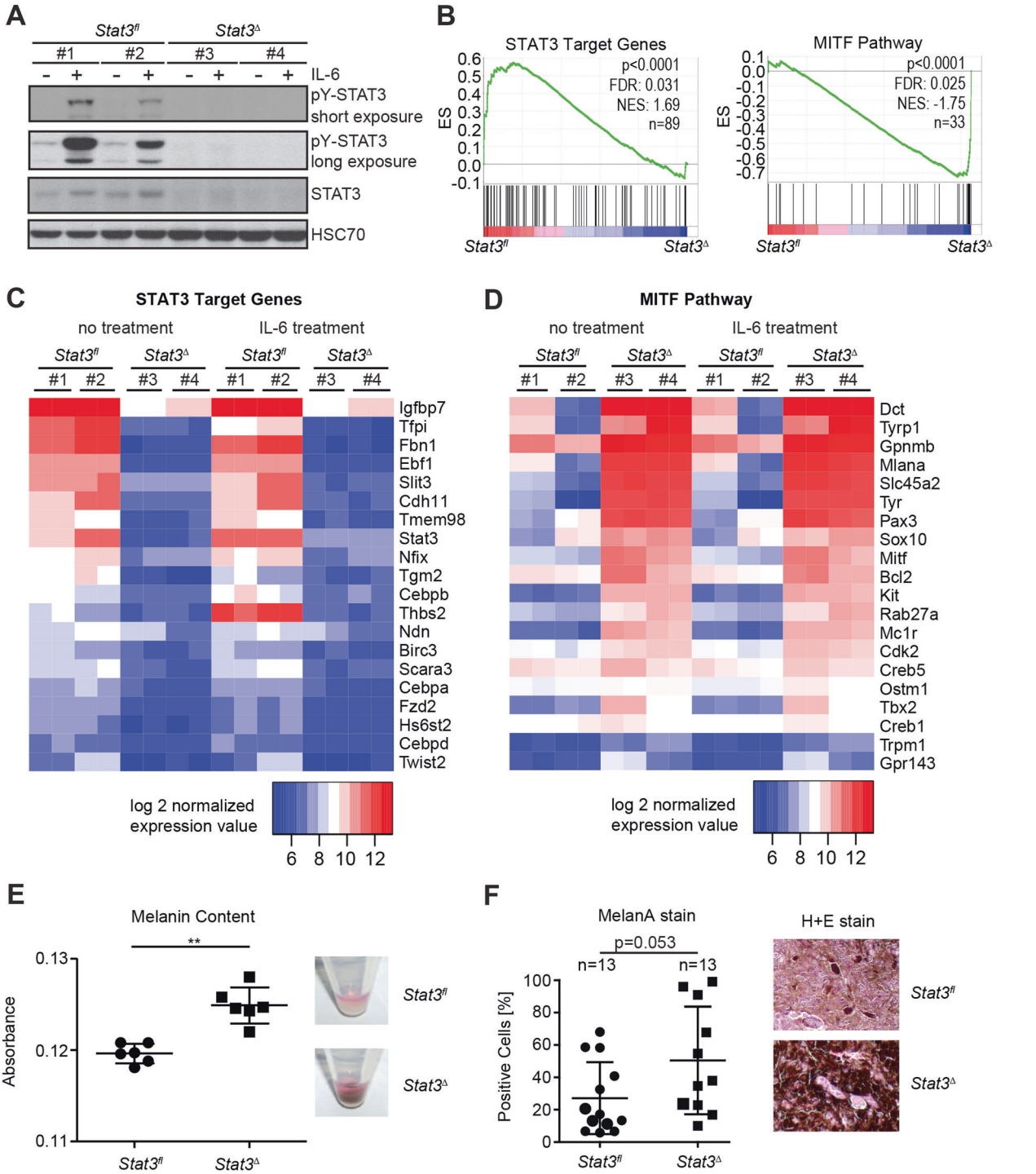

Fig. 2 Loss of *Stat3*-induced MITF pathway in melanoma cells. A Representative western blot showing total STAT3 levels and IL-6 stimulated (20 ng/ml, 30 min) STAT3 phosphorylation at Y705 in two representative cell lines derived from either Stat3^{fl} (#1 and #2) or Stat3$^{\Delta}$ tumors (#3 and #4). HSC70 served as loading control. **B** 89 STAT3 target genes and 33 genes in the MITF pathway were evaluated by gene-set enrichment analysis (GSEA) during normal growth in cell culture. **C** Heatmap showing the top 20 regulated genes of the STAT3 gene set. **D** Heatmap of the top 20 regulated genes of the MITF gene set. **E** Melanin content in supernatant from tumor-derived mouse melanoma cell lines, after 48 h of culturing, was measured by absorption at 410 nm. Results represent six independent measurements. **F** Tissue sections of primary tumors were stained by anti-MelanA antibody and percentage of positive cells is shown (left). Representative section, indicating melanin content, is shown (right). In (**E**, **F**) data are shown as mean ± SD. *P* values represent Mann–Whitney *U* test. $^{**}P < 0.01$.

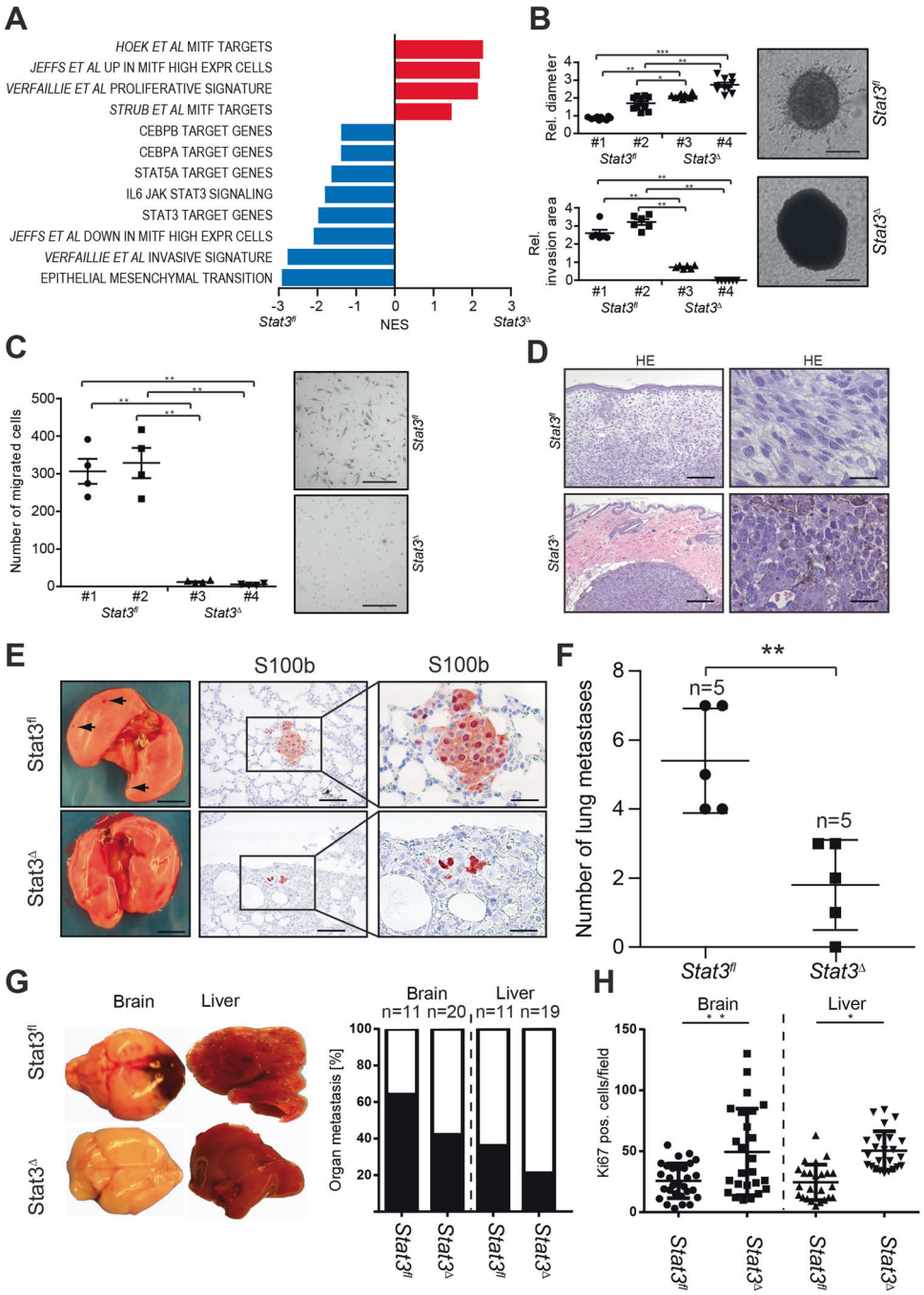

Fig. 3 Transcriptome analysis and functional testing revealed abrogated invasion and increased proliferation after STAT3 knockout. A Normalized enrichment scores (NES) calculated for gene signatures derived from the GSEA database (H and C3) or from publications (first author is listed) with a false discovery rate <5% and $P < 0.05$. **B** 3D proliferation and sphere invasion assay of Stat3^{fl} and Stat3$^{\Delta}$ melanoma cells into a collagen gel ($n = 10$/group). Stat3$^{\Delta}$ cells proliferate faster (upper panel) and have abrogated invasive capabilities ($n = 6$/group) (lower panel). Two representative spheres are displayed. Scale bar, 200 µm. **C** Transwell migration assay of Stat3^{fl} and Stat3$^{\Delta}$ melanoma cells ($n = 4$). STAT3 deletion leads to abrogated migration. Scale bar, 100 µm. **D** Representative HE stainings of tumors formed from Stat3^{fl} and Stat3$^{\Delta}$ cells grafted into NSG mice. Subcutaneously injected tumors of the Stat3^{fl} group invaded the dermis, while tumors of the Stat3$^{\Delta}$ group have a compact structure with even borders that did not invade into the dermis. Scale bar (left), 300 µm, scale bar (right), 20 µm. **E** Representative lungs, arrows indicate melanoma metastases (left); S100b staining (right). Scale bar (left), 3 mm, scale bar (middle), 150 µm, scale bar (right), 60 µm. **F** Metastasis quantification of age matched lung samples of Stat3^{fl} and Stat3$^{\Delta}$ mice, showing a total of 27 lung metastatic lesions in WT and 9 in KO mice. **G** Representative pictures for brain and liver metastasis (left). Distribution of organ metastasis in Stat3^{fl} and Stat3$^{\Delta}$ genotypes (right). **H** Total number of KI67 positive tumor cells per field of 500 tumor cells. Six individual tumor samples per genotype were analyzed in four random areas. In (**B**, **C**, **F**, **H**) data are shown as mean ± SD. *P* values represent Mann–Whitney *U* test. $*P < 0.05$; $**P < 0.01$; $***P < 0.001$.

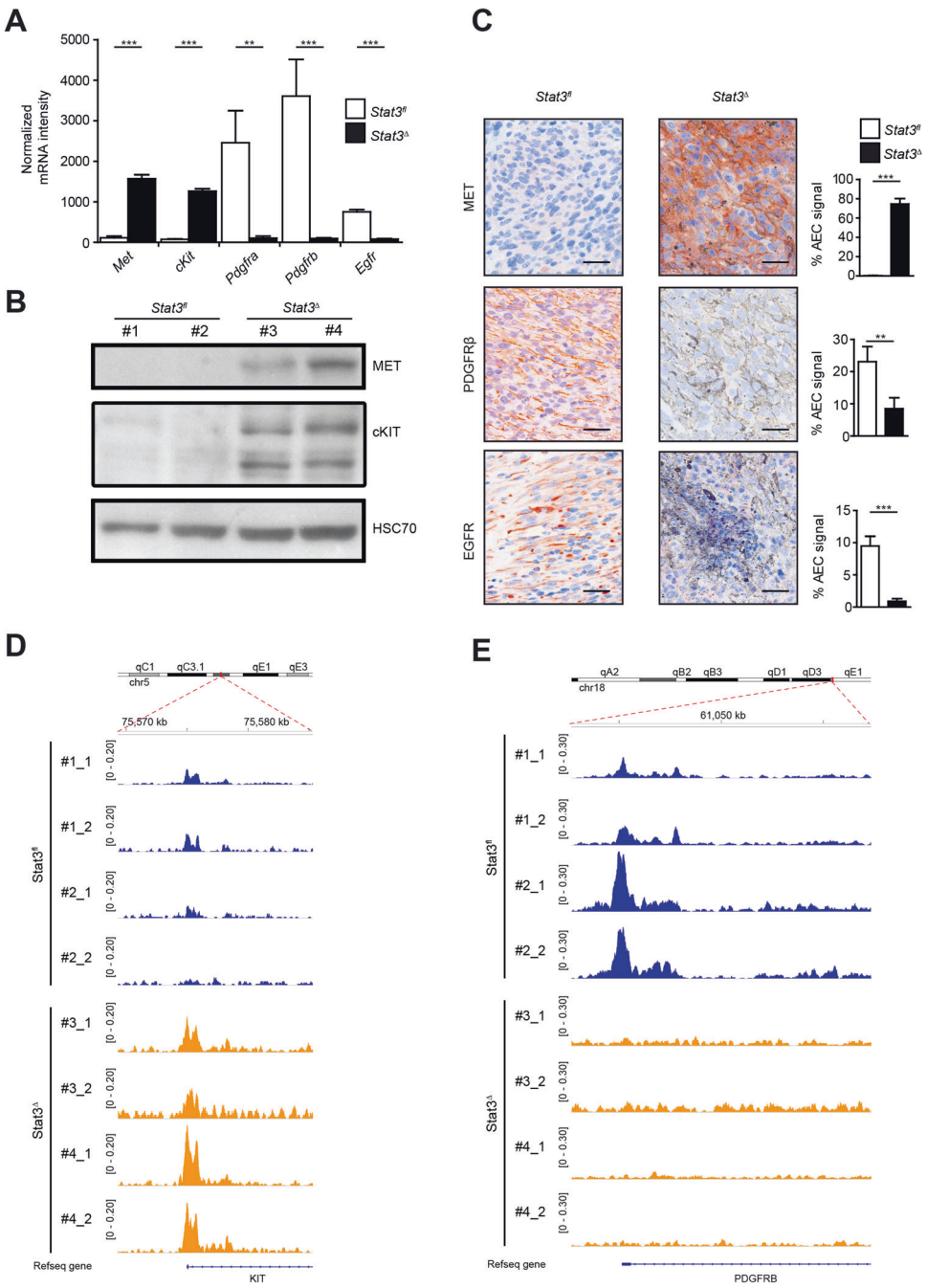

Fig. 4 Expression of receptor tyrosine kinases displays a YIN/YANG dualism corresponding to STAT3/MITF interplay. A The total mRNA levels of a set of significantly regulated RTK related to STAT3 and MITF signaling after normalization of the whole-transcriptome expression screen comparing the expression levels between the $Stat3^{fl}$ and the $Stat3^{\Delta}$ groups. Bar charts show mean expression intensity ± SD of six samples per group. **B** Western blot of two Stat3 wild type (#1 and #2) and two knockout cell lines (#3 and #4) for MET and cKIT. HSC70 served as loading control. **C** Representative images of antibody stainings in tumors derived of grafted $Stat3^{fl}$ and $Stat3^{\Delta}$ cell lines in NSG mice. Red color depicts specific immunostaining and black/brown is related to pigmentation. Scale bar, 25 µm. Bar charts showing AEC signal mean ± SD of four samples per group. **D**, **E** ATAC-seq signal intensities at the *cKit* and at the *Pdgfrb* locus. Two independent cell lines with biological duplicates are depicted in blue as $STAT3^{fl}$ and in yellow as $STAT3^{\Delta}$. *P* values represent Mann–Whitney *U* test. $*P < 0.05$; $**P < 0.01$; $***P < 0.001$.

Next, lungs of 40-week-old mice were stained for S100b to visualize metastasis formation. Importantly, *Stat3* deletion significantly reduced the overall number of metastatic lung colonies (Fig. 3E, F). Furthermore, we screened brains and livers from sacrificed animals for macroscopic tumor colonization. Brain metastasis was reduced by 23% and liver metastasis was reduced by 15% in the *Stat3* knockout animals (Fig. 3G). Additionally, we performed KI67 staining and identified a significant increase in labeling of metastatic lesions of knockout animals (Fig. 3H). In summary, knockout animals showed earlier onset of disease, increased PCNA expression in primary tumors and increased KI67 amounts in metastatic samples, but knockout cells also displayed decreased invasive capacities and less metastasis forming activity in distal organs. Next we asked how these different properties impact the overall survival of mice. Therefore we estimated the survival curve from cage side observations and the derived Kaplan–Meier plot showed that survival between both groups of animals was comparable (Supplementary Fig. S4). This indicated that although wild-type and knockout mice exhibited different phenotypes, in the end tumor burden, regarded as the

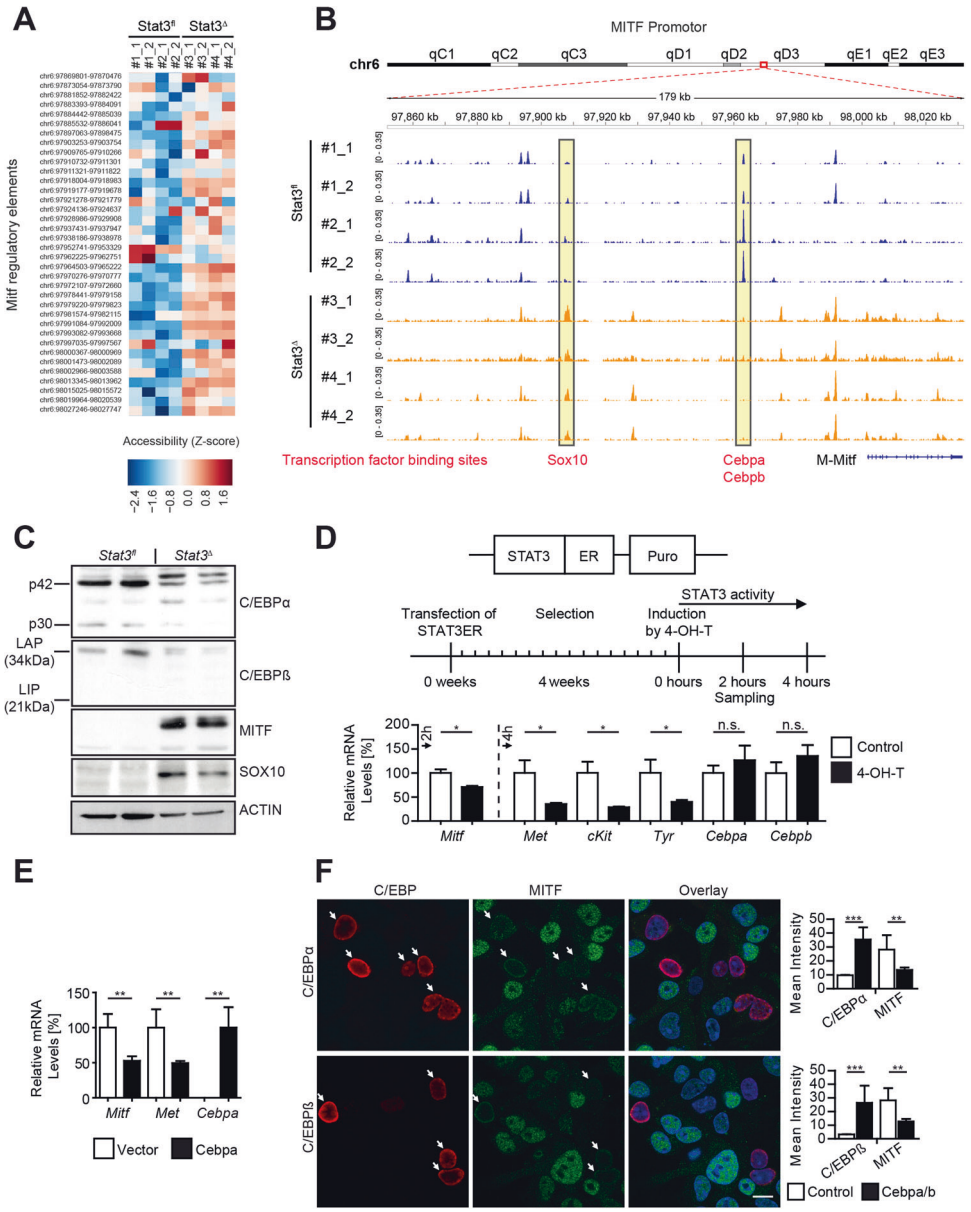

Fig. 5 MITF expression depends on the STAT3 target *Cebpa* and *Cebpb*. **A** Heatmap displays the grade of accessible chromatin from MITF regulatory elements. Blue correlates with closed or less accessible chromatin and red with open or more accessible chromatin for binding factors. **B** ATAC-seq signal intensities at the M-MITF locus and the possible binding sites of SOX10 and CEBPa/b. Data mapped according to ChIP-Atlas. Depicted in blue are $Stat3^{fl}$ cell lines and in yellow $Stat3^{\Delta}$ cell lines all in technical duplicates. **C** Western blots show increased expression of both the 42 kDa (p42) and the 30 kDa (p30) isoform of CEBPa/b and decreased expression of MITF and SOX10 in $Stat3^{fl}$ cells in comparison to the $Stat3^{\Delta}$ group. Actin served as loading control. **D** Lipofectamine transfection and stable selection via puromycin of $Stat3^{fl}$ murine melanoma cells with a $STAT3ER^{T2}$ construct that can be activated by 4-Hydroxytamoxifen (4-OH-T). MITF pathway is downregulated after two to 4 h after activation with 1 µM 4-OH-T. Bar charts show mean expression intensity ± SD of four samples per group **E** *Mitf* and *Met* regulation after 24 h transient *Cebpa* transfection of murine $Stat3^{\Delta}$ cells by lipofectamine. Bar charts show mean expression intensity ± SD of four samples per group. **F** Co-immunofluorescence for CEBPa or CEBPb and MITF expression after transient *Cebpa* or *Cebpb* transfection by lipofectamine for 24 h in $Stat3^{\Delta}$ murine melanoma cells. Scale bar, 5 µm. Quantification of cells expressing CEBPa or CEBPb by showing mean intensity ± SD of ten samples per group. *P* values represent Mann–Whitney *U* test. ns not significant. $*P < 0.05$; $**P < 0.01$; $***P < 0.001$.

sum of tumor spread and tumor growth, resulted in a similar outcome in life expectancy.

We continued to further analyze whole-genome expression profiling, which revealed a set of five important deregulated receptor tyrosine kinases. Three of them, *Platelet-Derived Growth Factor Receptor alpha and beta* (*PDGFRa/b*) and *Epidermal Growth Factor Receptor* (*EGFR*), displayed decreased mRNA expression in the

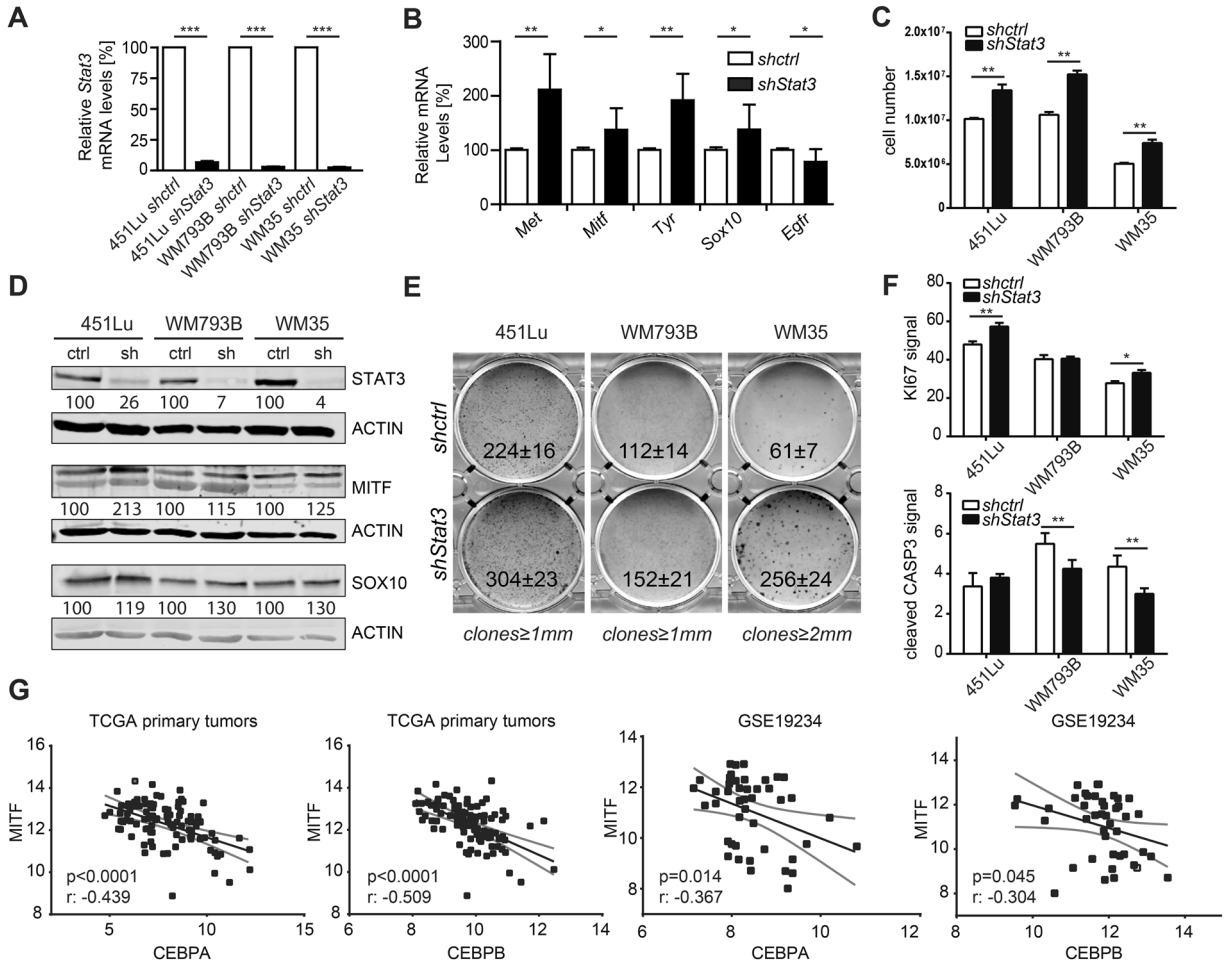

Fig. 6 Human melanoma cells induce MITF and proliferation upon loss of STAT3. Three human melanoma cell lines were transduced with *STAT3* shRNA or a scrambled control by lentivirus and selected via puromycin resistance. **A** Evaluation *STAT3* RNA amounts by RT-PCR. **B** mRNA expression of MITF pathway members was upregulated upon *STAT3* silencing in WM35 cells. **C** Of each cell line 10^6 cells were seeded and after 4 days of culturing cell number was measured. **D** Evaluation of the *shSTAT3* RNA knockdown by western blot for STAT3, SOX10, and MITF levels. Actin served as loading control. Numbers depict normalized intensity levels. **E** Of each cell line 10^4 cells were used for a clonogenic growth assay. After 10 days of growth colonies were fixed and stained with crystal violet. Three independent samples were counted, mean ± SD is shown. **F** Each line was seeded in 96-well plates and stained with anti-KI67 and anti-cleaved caspase 3 antibodies. Normalized fluorescence signals are shown. **G** Data from the publically available "the cancer genome atlas – skin cutaneous melanoma (TCGA-SKCM)" and "GSE19234" human malignant melanoma patient data sets (Bogunovic, TCGA) were tested for correlations between *CEBPA* vs. *MITF* and *CEBPB* vs. *MITF* by calculating Pearson correlation coefficients. Data in (**A**, **B**, **C**, **F**) are bar charts showing mean expression intensity ± SD of four samples per group. *P* values represent Mann–Whitney *U* test. $*P < 0.05$; $**P < 0.01$, $***P < 0.001$.

Stat3$^{\Delta}$ group (Fig. 4A and Supplementary Fig. S5). Two receptor tyrosine kinases, *MET* and *cKIT*, were increased (Fig. 4B). Accordingly, PDGFRb and EGFR were highly expressed in immunostainings of primary Stat3^{fl} mouse melanomas, whereas Stat3$^{\Delta}$ tumors showed increased expression of MET (Fig. 4C). PDGFRb and EGFR were also highly expressed in wild-type primary tumors, whereas MET was predominantly expressed in corresponding *Stat3* knockout samples (Supplementary Fig. S6).

To dissect the regulatory basis for the observed changes in the cell transcriptomes, we performed chromatin profiling using ATAC-seq with a focus on the *cKit* and *Pdgfrb* locus in Stat3^{fl} and Stat3$^{\Delta}$ melanoma cells. Chromatin accessibility at the *cKit* promoter region was increased only in Stat3$^{\Delta}$ and conversely the *Pdgfrb* promoter was only accessible in Stat3^{fl} cells (Fig. 4D, E). This indicates that the loss of STAT3 leads to epigenetic changes accompanied by the observed strong changes in gene expression patterns.

Assessment of chromatin accessibility reveals reciprocal expression between CEBPs and MITF

To investigate the mechanisms underlying the regulation of MITF by STAT3, we reasoned that STAT3 or its downstream

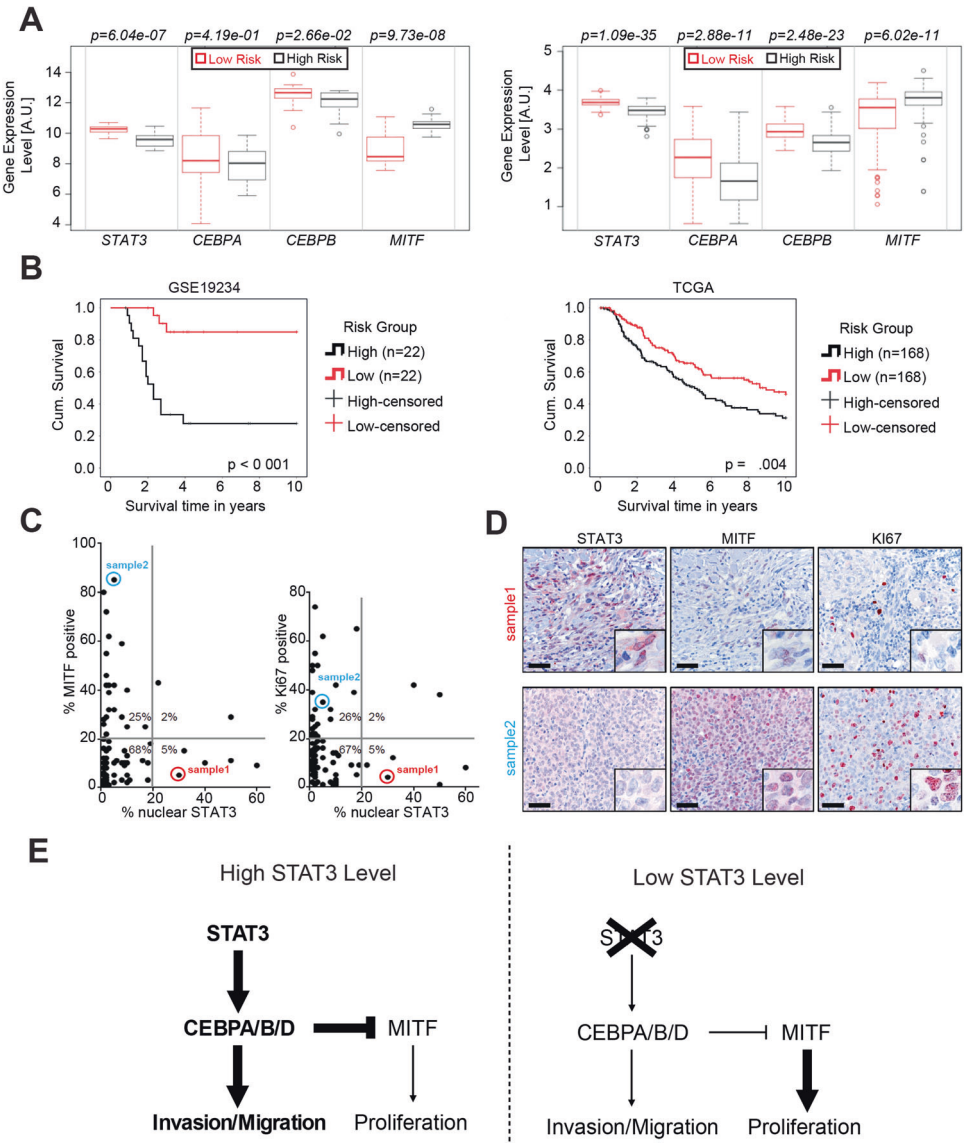

Fig. 7 Human patients with STAT3^{low}, CEBPA^{low}, CEBPB^{low}, and MITF^{high} signature show worsened clinical outcome. **A** Box–Whisker plot of mean gene expression levels of *STAT3*, *CEBPA*, *CEBPB*, and *MITF*, which were determined by survexpress to result in a maximum survival probability difference between low- and high-risk groups. Data sets were used from *Bogunovic* et al. (44 samples, GSE19234) and the TCGA-SKCM (336 samples). **B** Kaplan–Meier analysis of high- and low-risk groups as defined in (**A**). **C** A group of 98 melanoma metastasis samples was stained for STAT3, MITF, and KI67. Each sample was evaluated for the distribution of nuclear STAT3, as well as MITF and KI67. **D** Two representative tissue samples (sample1 for high nuclear STAT3 and sample2 for low nuclear STAT3) are shown with three consecutive sections, which were stained for STAT3, MITF, and KI67. Scale bars, 50 µm. **E** Scheme depicting changes in transcription factor interaction governing the melanoma phenotype. In Stat3^{fl} mice, STAT3 pathway is active, EGFR and PDGFRa/b are upregulated, and an EMT-like melanoma phenotype persists. When STAT3 activity is low or absent, MITF is released from suppression by CEBP family members. Subsequently, MITF target genes like *cKIT* and *MET* are upregulated and proliferation of melanoma is enhanced.

targets could repress MITF. To test this hypothesis, we investigated regulatory elements of the proximal *Mitf* promoter region by ATAC-seq. We found that Stat3^{fl} cells displayed chromatin accessibility in a regulatory element in close proximity of the *Mitf* gene, which contained a *CEBPa/b* binding element (Fig. 5A, B). Access at this site was specifically lost in Stat3$^{\Delta}$ cells. Contrary, Stat3$^{\Delta}$ cells displayed an increased accessibility at a regulatory element containing a *SOX10* binding element that was absent in Stat3^{fl} cells.

The CEBP transcription factors are well-known downstream targets of STAT3, and we could identify strong inhibition of *Cebpa/b/d* mRNA expression after *Stat3* knockout. Moreover, via protein analysis, we found significantly increased CEBPa/b in an STAT3-dependent way

and we could confirm reciprocal expression with MITF and SOX10 (Fig. 5C). Next, we introduced a 4-OH-tamoxifen inducible STAT3ER^{T2} construct [26] into Stat3$^{\Delta}$ murine melanoma cells. Addition of 4-OH-tamoxifen led to an increased expression of *Cebpa/b* mRNA as measured by RT-PCR analysis (Fig. 5D). Expression and activation of the STAT3ER^{T2} fusion protein by 4-OH-tamoxifen was confirmed by western blot analysis (Supplementary Fig. S7A). Induced STAT3 activity led to a reciprocal down-regulation of MITF pathway associated genes and *Mitf*, *Met*, *cKit*, *Tyr* were significantly repressed. Importantly, exogenous *Cebpa* expression in Stat3$^{\Delta}$ melanoma cells and subsequent mRNA quantification led to a significant reduction in *Mitf* and *Met* expression, altering levels of these genes to approximately 50% of control cells (Fig. 5E). To validate these findings CEBPa or CEBPb were ectopically overexpressed, and MITF expression was monitored on single cell level using microscopy. Melanoma cells devoid of STAT3 showed increased MITF protein expression, but when transfected with CEBPa or CEBPb then MITF levels where significantly reduced (Fig. 5F and Supplementary Figs. S7b and S8a, b). We conclude that STAT3-driven CEBP family member expression is responsible for repression of MITF mRNA and protein levels.

To test, whether our findings also apply for human melanoma cell lines, we performed stable lentiviral shRNA mediated knockdown of *Stat3* in 451Lu, WM793B, and WM35 cells. All three cell lines have the *INK4A* locus deleted and are driven by a BRAF^{V600E} mutation. Evaluation of the knockdown was performed via RT-PCR (Fig. 6A). Consistent with our murine data, we observed the upregulation of *MITF*, *MET*, *SOX10*, and *TYR* on mRNA level (Fig. 6B). Furthermore, cells devoid of *Stat3* showed increased cell proliferation (Fig. 6C). MITF and SOX10 were also upregulated on protein level (Fig. 6D). Additionally, increased clonogenic growth capabilities were observed (Fig. 6E). To discriminate whether the increase in cell number is due to increased cycling of cells or due to decreased apoptosis we quantified KI67 and cleaved caspase 3 amounts in the respective cell lines (Fig. 6F). To further validate and to address the clinical relevance of our findings, we evaluated publically available expression data sets from the Gene Expression Omnibus (GEO) and The Cancer Genome Atlas (TCGA) databases. This analysis revealed a strong negative correlation between *MITF* and *CEBPA* as well as between *MITF* and *CEBPB* expression (Fig. 6G).

Validation of STAT3 expression signatures in human clinical samples

To assess the clinical relevance of the relationship between MITF and CEBPa/b, we analyzed publicly available data sets (GEO accession GSE19234 and TCGA data from Cutaneous Melanoma). Using the online tool SurvExpress [27] samples were sorted according to the expression level of *STAT3*, *CEBPA*, *CEBPB*, and *MITF* to generate equal sized low- and high-risk groups, to achieve the maximum possible difference in estimate patient survival times (Fig. 7A). The high-risk group was defined by high levels of *MITF* in combination with low *STAT3*, *CEBPA*, and *CEBPB* levels. As expected, Kaplan–Meier survival analysis showed significant differences in survival probability between high- and low-risk groups in both cohorts (Fig. 7B). We also analyzed survival of patients based solely on STAT3 expression in the TCGA data set and patient cumulative survival is predicted with $P = 0.017$ (Supplementary Fig. S9a, b). To validate our findings in human patient samples, we analyzed a cohort of 25 primary melanoma tumors and 96–130 melanoma metastases for STAT3 and MITF antibody-mediated staining intensities. Primary tumors compared to metastases showed higher levels of STAT3 protein, while MITF levels were higher in metastases than in primary tumors (Supplementary Figs. S10a, b and S11). To indicate active STAT3, we focused on nuclear STAT3 localization, and we used consecutive sections to analyze co-occurring amounts of MITF and KI67 (Fig. 7C). Representative stained samples are shown (Fig. 7D).

In summary, we conclude that expression of CEBP family members depends on expression of STAT3 protein. Upon *Stat3* deletion, *Cebpa*, *Cebpb*, and *Cebpd* levels decrease, translating also in diminished protein expression and resulting in increased expression of MITF. This process leads to abrogated invasion and to diminished metastasis formation as illustrated in the summary schematic (Fig. 7E).

Discussion

We identified STAT3 as a critical regulator in the dynamic process of melanoma progression. Using a NRAS-driven mouse cutaneous melanoma model, devoid of INK4A tumor suppressors, we found that on the one hand STAT3 facilitated tumor cell spreading, while on the other hand STAT3 repressed MITF levels and it also diminished slightly proliferation of tumor cells. This indicates that STAT3 represents an important novel regulator in the complex relationship between phases of invasion and alternating phases of proliferation. Our findings have implications for the diagnosis as well as for therapeutic treatment of melanoma.

Tumor cells undergo progression and metastatic spread by adopting different biologic programs like proliferation, invasion, extravasation, and distant colonization known as the invasion-metastasis cascade [28]. During this process, the alteration of proliferative phases with low proliferative phases is of paramount importance [2]. Here we propose

that STAT3 is a key molecule able to regulate this transition. Analysis of STAT3 mutations in human solid cancers, including melanoma, revealed a low mutation frequency (28). Loss of function mutations like nonsense and frameshift mutations were even less frequent compared to missense mutations [29]. These data support the notion that STAT3 is not a major target for somatic mutations in solid tumors, but subjected to extensive upstream regulation. Hence, levels of STAT3 activity can change according to the cellular context and furthermore influence melanoma progression. Likewise tumor cells with active STAT3 are prone for increased invasion and metastasis, for example, at the invasive tumor boarder, while cells with downregulated or no STAT3 show enhanced proliferation, for example, at the metastatic site. Here, we provide evidence that genetic deletion of the *STAT3* locus reduces the plasticity of melanoma cells and inhibits the transition from a proliferative phenotype to an invasive phenotype.

We have shown that loss of STAT3 expression is accompanied with increased proliferation as loss of STAT3 caused an earlier disease onset in mice consistent with a pronounced proliferative signature marked by augmented MITF expression. In human cells, knockdown of STAT3 also resulted in the upregulation of MITF and induction of cell proliferation and this could be explained by STAT3 interfering with malignant melanoma growth through antagonizing MITF. When we further compare histology data from our mouse model with findings from our human study, we can observe that the increased cell proliferation in STAT3 knockout mouse tumors is reflected in elevated KI67 staining of human melanoma samples, which also show decreased STAT3 expression. Interestingly, increased labeling for KI67 as well as mitotic counts are robust prognostic predictors for worsening of survival in melanoma-bearing individuals [30, 31]. Both, our mouse and human studies show that tumors low in STAT3 display high amounts of MITF and importantly, metastatic melanoma patients with MITF amplifications show a dramatic decrease in survival probabilities compared to normal MITF status [32]. Hence, our bioinformatics analysis exemplifies that low amounts of STAT3 are associated with the so-called high-risk group, probably due to high proliferation, whereas melanoma cells high in STAT3 are low in proliferation and form the so-called low-risk group.

MITF is a master transcription factor during melanocytic differentiation and controls lineage-specific proliferation [33]. We suggest that the MITF repression is mediated by increased CEBPA and CEBPB amounts. CEBP family members are well-established downstream targets of STAT3 [34]. Binding of SOX10 to the MITF promoter positively regulates expression [35, 36], while binding of CEBPA inhibits MITF expression in myeloid cells [37]. Here we show that rescuing of $Stat3^{\Delta}$ melanoma cells by reactivation of the STAT3 pathway or by forced expression of *CEBPa/b* also repressed *Mitf* mRNA production. Furthermore, we show that the loss of STAT3 diminished expression of CEBP family members, and CEBP binding motifs were less accessible as determined by ATAC-seq at the *Mitf* locus. Analysis of human expression data sets showed that high *MITF* correlated with low *STAT3* and *CEBPa/b* levels.

We have shown that STAT3 was essential for the establishment of an EMT signature according to whole-genome expression profiling. Tumor invasion and migration activity were abrogated upon STAT3 loss, reminiscent of a loss of an EMT-like phenotype. Additionally, we found EGFR and PDGFR upregulation in wild type compared to STAT3 knockout melanomas. PDGFR-beta is, for example, strongly expressed in pericytes, and its expression in epithelial cells is regarded as a marker for the EMT phenotype [38]. Our conclusion regarding STAT3 as a metastasis driver is strengthened by recent reports, which describe STAT3 activity in melanoma cells as a driver for upregulation of invasion-related genes and as a major factor in the transition toward a mesenchymal phenotype during EMT-like processes [39]. Additionally, DNp73 was shown to initiate metastasis in melanoma by activating STAT3 signaling [40]. Likewise, STAT3 was also shown to drive pancreas cancer metastasis to the liver [41], and STAT3 inhibition served as an effective strategy to reduce invasion and migration of cells [12, 42].

The presence of an EMT phenotype has not only been associated with invasion and migration, but also with an increased stemness of tumor cells [43]. Interestingly, STAT3 controls stability of NANOG and SOX2, which are important stem cells transcription factors [44, 45]. STAT3 is also required for the viability of cancer stem cells in different tumor types including melanoma [46–49].

Treatment of melanoma currently focuses on the use of BRAF and MEK inhibitors, as well as on the remarkable success with blockade of immune checkpoint inhibitors. Unfortunately patients still show low response rates toward anti-melanoma therapy, which has been attributed to the pronounced EMT-like phenotype [50, 51]. Specifically, EMT in tumor patients is considered as a major factor in the development of resistance toward tyrosine kinase blockers [4] and for escaping PD-1 immunotherapy treatment [52]. Mechanistically resistance to vemurafenib treatment can occur when patients are low in MITF which leads, in line with our data, to corresponding upregulation of EGFR [53]. Therefore, involvement of STAT3 in the EMT process, in enhancing stemness, as well as in immune evasion phenotype of tumor cells, could have significant implications for future melanoma therapy.

Our human STAT3 melanoma data pinpoint to a possible novel therapeutic opportunity. Hence, we suggest that targeting of STAT3 would prevent repetitive switching of

tumor cells into an invasive, low proliferative, and more treatment resistant cell population. To counteract the rise in proliferation after STAT3 inhibition a combinatory treatment approach to also suppress MITF can be envisioned. This could be achieved by interfering with tumor differentiation or by decreasing the levels of SR-BI in melanoma [54, 55]. Already in clinical use are HDAC inhibitors, which also show suppression of MITF [56]. Therefore, panobinostat and vorinostat are candidate drugs, currently being tested as adjuvant therapy (NCT02032810), or as stand-alone treatment (NCT02836548) after $BRAF^{V600E}$ inhibitor resistance (data from clinicaltrials.gov). Additionally, clinically approved tyrosine kinase inhibitors such as Dasatinib and Nilotinib, inhibiting cKIT/PDGFR, or Crizotinib and Cabozantinib, inhibiting cMET/ALK, could be used in combination with STAT3 inhibition.

Our findings imply that STAT3 represents a vulnerable node enabling melanoma transition from proliferation to migration and invasion. We conclude that a balanced expression of STAT3 and MITF controls melanoma fate, and we propose that the main role of STAT3 is to promote invasion and metastatic spread.

Materials and methods

Animals

Mice carrying the *Stat3*^{floxed} allele [21] were crossed with transgenic mice carrying melanocyte-specific expression of the *NRAS*^{Q61K} oncogene in an INK4A-deficient background [19, 57] and tyrosinase *Cre* [58]. Human *NRAS*^{Q61K} and *Cre* are targeted to the melanocyte linage by tyrosinase regulatory sequences. Compound *Tyr::NRAS*^{Q61K} *Ink4a*$^{-/-}$; *Stat3*$^{flox/flox}$; *Tyr::Cre* mice were termed Stat3$^{\Delta}$ for simplified reading and maintained on a C57BL/6Jx129/Sv background. In all experiments described, sex ratio was equal, and littermates lacking *Tyr::Cre* were used as controls and termed Stat3^{fl}. For in vivo experiments the number of biological replicates is indicated in each figure shown. Animals were randomly assigned to groups, no blinding was applied. All mice were bred and maintained under standardized conditions at the Decentralized Biomedical Facility of the Medical University Vienna according to an ethical animal license protocol complying with the Austrian law and approved by the "Bundesministerium für Wissenschaft und Forschung" (BMWF-66009/0281-I/3b/2012).

Cell lines

Mouse melanoma cell lines were established from lymph nodes of diseased mice (25–30 weeks of age) by single cell dissociation and culturing. Multiple individual primary pools of cell lines per Stat3^{fl} and Stat3$^{\Delta}$ melanoma cell genotype were generated, upon which we selected two pools each for further detailed analysis. Gene lists for STAT3 targets are shown in Supplementary Table 1, and the MITF pathway members are shown in Supplementary Table 2. The primers used in this study are listed in Supplementary Table 3. Human *BRAF*-mutated cell lines WM793B, 451Lu, and WM35 were freshly bought from ATCC. All cell lines were cultivated under standard conditions (95% humidity, 5% CO_2, 37 °C) and maintained in DMEM supplied with 10% Fetal Bovine Serum, 10 U/ml Penicillin, 10 µg/ml Streptomycin, 2 mM L-Glutamine (all from Gibco, Thermo Fisher, Waltham, MA), and 2 µg/ml Ciprofloxacin (Sigma-Aldrich, St. Louis, MO). Cell lines were routinely tested for mycoplasma contamination.

Immunohistochemistry and immunofluorescence

For immunohistochemistry, 4 µm tissue sections were deparaffinized and rehydrated in graded ethanol dilutions, after which antigen retrieval was carried out. Staining was performed using the ABC kit according to the manufacturer's instructions (Novocastra, Wetzlar, Germany). As substrate 3-amino-9-ethylcarbazole was used (Agilent Technologies) and imaging was done with an Olympus BX63 microscope. The intensity of staining was evaluated by two blinded, board-certified pathologists. For immunofluorescence cells were grown on chamber slides and fixed in 4% formaldehyde. After staining with primary and corresponding secondary antibodies imaging was done on a Leica TCS SP8 Microscope. Signal intensity was calculated by measuring pixel density in ImageJ for CEBP positive nuclei and control nuclei. The antibodies used in this study are listed in Supplementary Tables 4 and 5. Full size western blots are shown in Supplementary Fig. 1a–d.

Clinical samples

All melanoma samples were obtained from the Department of Dermatology, General Hospital Vienna. In each case, pathological diagnosis was made after elective surgery for malignant melanoma. Human tissue samples were collected after signed, informed consent was provided and approval for studies was obtained from Ethics Committee of the Medical University of Vienna, EK 405/2006, extension 11/10/2016. Additional "Materials and Methods" are provided in Supplementary Information.

Acknowledgements We thank Safia Zahma, Birgit Schütz, Eva Bauer, Michaela Schlederer, and Karin Neumüller for excellent technical assistance. We also thank the Biomedical Sequencing Facility at CeMM for assistance with next-generation sequencing. VP was supported by the grant AIRC IG16930, AS, OE, RZ, and RM were supported by a private melanoma research donation from

Liechtenstein, RM was further supported by two network grants SFB-F061 and SFB-F047, and RS, KK, MV, and MM were supported by P 25336-B13, all from the Austrian Science Fund (FWF).

Compliance with ethical standards

Conflict of interest The authors declare that they have no conflict of interest.

Publisher's note Springer Nature remains neutral with regard to jurisdictional claims in published maps and institutional affiliations.

References

1. Siegel RL, Miller KD, Jemal A. Cancer statistics, 2016. CA Cancer J Clin. 2016;66:7–30.
2. Hoek KS, Eichhoff OM, Schlegel NC, Dobbeling U, Kobert N, Schaerer L, et al. In vivo switching of human melanoma cells between proliferative and invasive states. Cancer Res. 2008;68:650–6.
3. Kemper K, de Goeje PL, Peeper DS, van Amerongen R. Phenotype switching: tumor cell plasticity as a resistance mechanism and target for therapy. Cancer Res. 2014;74:5937–41.
4. Li FZ, Dhillon AS, Anderson RL, McArthur G, Ferrao PT. Phenotype switching in melanoma: implications for progression and therapy. Front Oncol. 2015;5:31.
5. Yasumoto K, Yokoyama K, Shibata K, Tomita Y, Shibahara S. Microphthalmia-associated transcription factor as a regulator for melanocyte-specific transcription of the human tyrosinase gene. Mol Cell Biol. 1994;14:8058–70.
6. Hemesath TJ, Steingrimsson E, McGill G, Hansen MJ, Vaught J, Hodgkinson CA, et al. microphthalmia, a critical factor in melanocyte development, defines a discrete transcription factor family. Genes Dev. 1994;8:2770–80.
7. Steingrimsson E, Copeland NG, Jenkins NA. Melanocytes and the microphthalmia transcription factor network. Annu Rev Genet. 2004;38:365–411.
8. Carreira S, Goodall J, Denat L, Rodriguez M, Nuciforo P, Hoek KS, et al. Mitf regulation of Dia1 controls melanoma proliferation and invasiveness. Genes Dev. 2006;20:3426–39.
9. Goodall J, Carreira S, Denat L, Kobi D, Davidson I, Nuciforo P, et al. Brn-2 represses microphthalmia-associated transcription factor expression and marks a distinct subpopulation of microphthalmia-associated transcription factor-negative melanoma cells. Cancer Res. 2008;68:7788–94.
10. Verfaillie A, Imrichova H, Atak ZK, Dewaele M, Rambow F, Hulselmans G, et al. Decoding the regulatory landscape of melanoma reveals TEADS as regulators of the invasive cell state. Nat Commun. 2015;6:6683.
11. Kortylewski M, Jove R, Yu H. Targeting STAT3 affects melanoma on multiple fronts. Cancer Metastasis Rev. 2005;24:315–27.
12. Fofaria NM, Srivastava SK. Critical role of STAT3 in melanoma metastasis through anoikis resistance. Oncotarget. 2014;5:7051–64.
13. Niu G, Heller R, Catlett-Falcone R, Coppola D, Jaroszeski M, Dalton W, et al. Gene therapy with dominant-negative Stat3 suppresses growth of the murine melanoma B16 tumor in vivo. Cancer Res. 1999;59:5059–63.
14. Kortylewski M, Heinrich PC, Mackiewicz A, Schniertshauer U, Klingmuller U, Nakajima K, et al. Interleukin-6 and oncostatin M-induced growth inhibition of human A375 melanoma cells is STAT-dependent and involves upregulation of the cyclin-dependent kinase inhibitor p27/Kip1. Oncogene. 1999;18:3742–53.
15. Lacreusette A, Nguyen JM, Pandolfino MC, Khammari A, Dreno B, Jacques Y, et al. Loss of oncostatin M receptor beta in metastatic melanoma cells. Oncogene. 2007;26:881–92.
16. Grabner B, Schramek D, Mueller KM, Moll HP, Svinka J, Hoffmann T, et al. Disruption of STAT3 signalling promotes KRAS-induced lung tumorigenesis. Nat Commun. 2015;6:6285.
17. Musteanu M, Blaas L, Mair M, Schlederer M, Bilban M, Tauber S, et al. Stat3 is a negative regulator of intestinal tumor progression in Apc(Min) mice. Gastroenterology. 2010;138:1003–11.e1-5.
18. Pencik J, Schlederer M, Gruber W, Unger C, Walker SM, Chalaris A, et al. STAT3 regulated ARF expression suppresses prostate cancer metastasis. Nat Commun. 2015;6:7736.
19. Ackermann J, Frutschi M, Kaloulis K, McKee T, Trumpp A, Beermann F. Metastasizing melanoma formation caused by expression of activated N-RasQ61K on an INK4a-deficient background. Cancer Res. 2005;65:4005–11.
20. Cancer Genome Atlas Network. Genomic classification of cutaneous melanoma. Cell. 2015;161:1681–96.
21. Alonzi T, Maritano D, Gorgoni B, Rizzuto G, Libert C, Poli V. Essential role of STAT3 in the control of the acute-phase response as revealed by inducible gene inactivation [correction of activation] in the liver. Mol Cell Biol. 2001;21:1621–32.
22. Luciani F, Champeval D, Herbette A, Denat L, Aylaj B, Martinozzi S, et al. Biological and mathematical modeling of melanocyte development. Development. 2011;138:3943–54.
23. Jeffs AR, Glover AC, Slobbe LJ, Wang L, He S, Hazlett JA, et al. A gene expression signature of invasive potential in metastatic melanoma cells. PLoS ONE. 2009;4:e8461.
24. Strub T, Giuliano S, Ye T, Bonet C, Keime C, Kobi D, et al. Essential role of microphthalmia transcription factor for DNA replication, mitosis and genomic stability in melanoma. Oncogene. 2011;30:2319–32.
25. Subramanian A, Tamayo P, Mootha VK, Mukherjee S, Ebert BL, Gillette MA, et al. Gene set enrichment analysis: a knowledge-based approach for interpreting genome-wide expression profiles. Proc Natl Acad Sci USA. 2005;102:15545–50.
26. Matsuda T, Nakamura T, Nakao K, Arai T, Katsuki M, Heike T, et al. STAT3 activation is sufficient to maintain an undifferentiated state of mouse embryonic stem cells. EMBO J. 1999;18:4261–9.
27. Aguirre-Gamboa R, Gomez-Rueda H, Martinez-Ledesma E, Martinez-Torteya A, Chacolla-Huaringa R, Rodriguez-Barrientos A, et al. SurvExpress: an online biomarker validation tool and database for cancer gene expression data using survival analysis. PLoS ONE. 2013;8:e74250.
28. Lambert AW, Pattabiraman DR, Weinberg RA. Emerging biological principles of metastasis. Cell. 2017;168:670–91.
29. Igelmann S, Neubauer HA, Ferbeyre G. STAT3 and STAT5 activation in solid cancers. Cancers (Basel). 2019;11:1428–19.
30. Ladstein RG, Bachmann IM, Straume O, Akslen LA. Ki-67 expression is superior to mitotic count and novel proliferation markers PHH3, MCM4 and mitosin as a prognostic factor in thick cutaneous melanoma. BMC Cancer. 2010;10:140.
31. Tu TJ, Ma MW, Monni S, Rose AE, Yee H, Darvishian F, et al. A high proliferative index of recurrent melanoma is associated with worse survival. Oncology. 2011;80:181–7.
32. Garraway LA, Widlund HR, Rubin MA, Getz G, Berger AJ, Ramaswamy S, et al. Integrative genomic analyses identify MITF as a lineage survival oncogene amplified in malignant melanoma. Nature. 2005;436:117–22.
33. Goding CR, Arnheiter H. MITF-the first 25 years. Genes Dev. 2019;33:983–1007.
34. Yamada T, Tobita K, Osada S, Nishihara T, Imagawa M. CCAAT/enhancer-binding protein delta gene expression is mediated by APRF/STAT3. J Biochem. 1997;121:731–8.

35. Lee M, Goodall J, Verastegui C, Ballotti R, Goding CR. Direct regulation of the microphthalmia promoter by Sox10 links Waardenburg-Shah syndrome (WS4)-associated hypopigmentation and deafness to WS2. J Biol Chem. 2000;275:37978–83.
36. Verastegui C, Bille K, Ortonne JP, Ballotti R. Regulation of the microphthalmia-associated transcription factor gene by the Waardenburg syndrome type 4 gene, SOX10. J Biol Chem. 2000;275:30757–60.
37. Qi X, Hong J, Chaves L, Zhuang Y, Chen Y, Wang D, et al. Antagonistic regulation by the transcription factors C/EBPalpha and MITF specifies basophil and mast cell fates. Immunity. 2013;39:97–110.
38. Shenoy AK, Jin Y, Luo H, Tang M, Pampo C, Shao R, et al. Epithelial-to-mesenchymal transition confers pericyte properties on cancer cells. J Clin Invest. 2016;126:4174–86.
39. Ohanna M, Cheli Y, Bonet C, Bonazzi VF, Allegra M, Giuliano S, et al. Secretome from senescent melanoma engages the STAT3 pathway to favor reprogramming of naive melanoma towards a tumor-initiating cell phenotype. Oncotarget. 2013;4:2212–24.
40. Steder M, Alla V, Meier C, Spitschak A, Pahnke J, Furst K, et al. DNp73 exerts function in metastasis initiation by disconnecting the inhibitory role of EPLIN on IGF1R-AKT/STAT3 signaling. Cancer Cell. 2013;24:512–27.
41. Lee JW, Stone ML, Porrett PM, Thomas SK, Komar CA, Li JH, et al. Hepatocytes direct the formation of a pro-metastatic niche in the liver. Nature. 2019;567:249–52.
42. Cao HH, Chu JH, Kwan HY, Su T, Yu H, Cheng CY, et al. Inhibition of the STAT3 signaling pathway contributes to apigenin-mediated anti-metastatic effect in melanoma. Sci Rep. 2016;6:21731.
43. Weidenfeld K, Barkan D. EMT and stemness in tumor dormancy and outgrowth: are they intertwined processes? Front Oncol. 2018;8:381.
44. Tang Y, Luo Y, Jiang Z, Ma Y, Lin CJ, Kim C, et al. Jak/Stat3 signaling promotes somatic cell reprogramming by epigenetic regulation. Stem Cells. 2012;30:2645–56.
45. Huser L, Sachindra S, Granados K, Federico A, Larribere L, Novak D, et al. SOX2-mediated upregulation of CD24 promotes adaptive resistance toward targeted therapy in melanoma. Int J Cancer. 2018;143:3131–42.
46. Gong AH, Wei P, Zhang S, Yao J, Yuan Y, Zhou AD, et al. FoxM1 drives a feed-forward STAT3-activation signaling loop that promotes the self-renewal and tumorigenicity of glioblastoma stem-like cells. Cancer Res. 2015;75:2337–48.
47. He W, Wu J, Shi J, Huo YM, Dai W, Geng J, et al. IL22RA1/STAT3 signaling promotes stemness and tumorigenicity in pancreatic cancer. Cancer Res. 2018;78:3293–305.
48. Tang Y, Kitisin K, Jogunoori W, Li C, Deng CX, Mueller SC, et al. Progenitor/stem cells give rise to liver cancer due to aberrant TGF-beta and IL-6 signaling. Proc Natl Acad Sci USA. 2008;105:2445–50.
49. Kulesza DW, Przanowski P, Kaminska B. Knockdown of STAT3 targets a subpopulation of invasive melanoma stem-like cells. Cell Biol Int. 2019;43:613–22.
50. Anastas JN, Kulikauskas RM, Tamir T, Rizos H, Long GV, von Euw EM, et al. WNT5A enhances resistance of melanoma cells to targeted BRAF inhibitors. J Clin Invest. 2014;124:2877–90.
51. Kudo-Saito C, Shirako H, Takeuchi T, Kawakami Y. Cancer metastasis is accelerated through immunosuppression during Snail-induced EMT of cancer cells. Cancer Cell. 2009;15:195–206.
52. Bu X, Mahoney KM, Freeman GJ. Learning from PD-1 resistance: new combination strategies. Trends Mol Med. 2016;22:448–51.
53. Ji Z, Erin Chen Y, Kumar R, Taylor M, Jenny Njauw CN, Miao B, et al. MITF modulates therapeutic resistance through EGFR signaling. J Invest Dermatol. 2015;135:1863–72.
54. Mirea MA, Eckensperger S, Hengstschlager M, Mikula M. Insights into differentiation of melanocytes from human stem cells and their relevance for melanoma treatment. Cancers (Basel). 2020;12:2508–19.
55. Kinslechner K, Schutz B, Pistek M, Rapolter P, Weitzenbock HP, Hundsberger H. et al. Loss of SR-BI down-regulates MITF and suppresses extracellular vesicle release in human melanoma. Int J Mol Sci. 2019;20:1063–12.
56. Yokoyama S, Feige E, Poling LL, Levy C, Widlund HR, Khaled M, et al. Pharmacologic suppression of MITF expression via HDAC inhibitors in the melanocyte lineage. Pigment Cell Melanoma Res. 2008;21:457–63.
57. Serrano M, Lee H, Chin L, Cordon-Cardo C, Beach D, DePinho RA. Role of the INK4a locus in tumor suppression and cell mortality. Cell. 1996;85:27–37.
58. Delmas V, Martinozzi S, Bourgeois Y, Holzenberger M, Larue L. Cre-mediated recombination in the skin melanocyte lineage. Genesis. 2003;36:73–80.

Affiliations

Alexander Swoboda[1,2] · Robert Soukup[3] · Oliver Eckel[2,3] · Katharina Kinslechner[3] · Bettina Wingelhofer[1,2] · David Schörghofer[3] · Christina Sternberg[4] · Ha T. T. Pham[1,2] · Maria Vallianou[3] · Jaqueline Horvath[1,5] · Dagmar Stoiber[1,5] · Lukas Kenner[1,6,7,8] · Lionel Larue[9] · Valeria Poli[10] · Friedrich Beermann[11] · Takashi Yokota[12] · Stefan Kubicek[13] · Thomas Krausgruber[13] · André F. Rendeiro[13] · Christoph Bock[13,14,15] · Rainer Zenz[16] · Boris Kovacic[3] · Fritz Aberger[4] · Markus Hengstschläger[3] · Peter Petzelbauer[17] · Mario Mikula[3] · Richard Moriggl[1,2]

1 Ludwig Boltzmann Institute for Cancer Research, Vienna, Austria

2 Institute of Animal Breeding and Genetics, University of Veterinary Medicine, Vienna, Austria

3 Center for Pathobiochemistry and Genetics, Institute of Medical Genetics, Medical University of Vienna, Vienna, Austria

4 Department of Biosciences, Cancer Cluster Salzburg, University of Salzburg, Salzburg, Austria

5 Institute of Pharmacology, Center of Physiology and Pharmacology, Medical University of Vienna, Vienna, Austria

6 Institute of Clinical Pathology, Medical University of Vienna, Vienna, Austria

7 Unit of Pathology of Laboratory Animals, University of Veterinary Medicine, Vienna, Austria

[8] CBMed Core Lab2, Medical University of Vienna, Vienna, Austria

[9] Institute Curie, Normal and Pathological Development of Melanocytes, CNRS UMR3347, INSERM U1021 Equipe labellisée, Orsay, France

[10] Department of Molecular Biotechnology and Health Sciences, University of Torino, Turin, Italy

[11] ISREC, Swiss Federal Institute of Technology in Lausanne, Lausanne, Switzerland

[12] Department of Stem Cell Biology, Graduate School of Medical Sciences, Kanazawa University, Kanazawa, Ishikawa, Japan

[13] CeMM Research Center for Molecular Medicine of the Austrian Academy of Sciences, Vienna, Austria

[14] Department of Laboratory Medicine, Medical University of Vienna, Vienna, Austria

[15] Max Planck Institute for Informatics, Saarland Informatics Campus, Saarbrücken, Germany

[16] Institute of Cancer Research, Medical University of Vienna, Vienna, Austria

[17] Department of Dermatology, Skin and Endothelium Research Division (SERD), Medical University of Vienna, Vienna, Austria